

Slope Traversal Experiments with Slip Compensation Control for Lunar/Planetary Exploration Rover

Genya Ishigami, Keiji Nagatani, and Kazuya Yoshida

Abstract—This paper presents slope traversal experiments with slip compensation control for lunar/planetary exploration rovers. On loose soil, wheels of the rover easily slip even when the rover travels with relatively low velocity. Because of the slip, following an arbitrary path on loose soil becomes a difficult task for the rover, and also, the slip will increase when the rover traverses a slope. To cope with the slip issue, the authors previously proposed path following control strategy taking wheel slippages into account. Through numerical simulations in the previous work, it has been confirmed that the proposed control effectively compensates and reduces the slip motions of the rover, and then, the rover can follow a given path. In order to confirm the usefulness of the proposed control for practical application, slope traversal experiments using a four-wheeled rover test bed are addressed in this paper. The control performance of the slip compensation is compared to that of no slip control based on motion traces of the rover in side slope traversal case. Further, the effectiveness of the proposed control is verified by quantitative evaluations of distance and orientation errors.

I. INTRODUCTION

The surface of a planetary body, such as the Moon or Mars, is almost covered with loose soil. One particular concern on such loose soil is that the wheels of the rover can easily slip and get stuck. As reported by the Mars Exploration Rovers, Spirit and Opportunity [1], this wheel slippage is a major disturbance for their mobility. In addition, a sideslip of vehicle body is also another concern which will make a performance of path following control worse. Therefore, it is important issue to manage these slips to achieve path following tasks on loose soil.

There are a number of papers and books regarding path following issues [2]-[4]. For example, Rezaei et al. investigated an on-line path following strategy combined with a SLAM algorithm for a car-like robot in outdoor environments [3]. Helmick et al. developed a path following algorithm with slip compensation using visual odometry and a Kalman filter [4].

The mechanics of a slipping wheel on loose soil has been studied in the field of *Terramechanics* [5]-[8]. In this field, the principle of the wheel-soil interaction mechanics and the empirical models of the stress distribution beneath the wheel have been investigated, as in [5], [6]. Iagnemma et al. applied these classical models to modern issues of planetary rovers [7]. The present authors have also elaborated upon the

wheel-and-vehicle model to address traveling performances of rovers with slipping wheels [8].

By employing our background regarding the slip motion, a path following control strategy with slip compensation on loose soil has been developed in our previous research, as in [9]. A key approach of the control is to compensate three types of slip, namely vehicle's sideslip and both longitudinal and lateral slips of wheel. Based on the proposed control, both steering and driving maneuvers of rover are derived such that three types of slips are successfully compensated as well as the rover can follow an arbitrary path. The performance of this path following control was confirmed through dynamic simulations. This control strategy, however, have not been demonstrated by experimental tests and then relevance for practical application was left as an open issue.

In this paper, to confirm the usefulness of our proposed control for the practical application, slope traversal experiments using a four-wheeled rover test bed are described. Experiments are conducted using a tiltable test field with giving different side slope inclinations. The practical performance of the proposed control is compared to the no slip control based on motion traces of the rover in side slope traversal experiments. Further, the effectiveness of the proposed control is verified by quantitative evaluations of distance and orientation errors. In addition, several potential issues indicated from the experimental results are discussed in order to further enhance the usefulness of the slip compensation control for practical applications,

The paper is organized as follows: Section II presents the proposed technique for the slip compensation control. Derivation of both steering and driving maneuvers are formulated in Section III along with a nonholonomic kinematic model of the vehicle taking into account the slips. In Section IV, the slope traversal experiments are described and then the performance of the proposed control is evaluated.

II. SLIP COMPENSATION CONTROL

A. Problem Statement

When a rover traverses on a side slope of loose sand, the vehicle body of the rover experiences a sideslip, which is measured by slip angle. As shown in Fig. 1, the slip angle of the vehicle, β_0 , is calculated by using the longitudinal and lateral linear velocities on the vehicle coordinate, v_x and v_y , as follows:

$$\beta_0 = \tan^{-1}(v_y/v_x) \quad (1)$$

Based on the kinematics and terramechanics, non-zero slip angle also occurs due to cornering effect coupled with

This work was supported in part by Research Fellowships of the Japan Society for the Promotion of Science for Young Scientists.

The authors are with Department of Aerospace Engineering, Tohoku University, Aoba 6-6-01, Sendai, 980-8579, Japan, {ishigami,keiji,yoshida}@astro.mech.tohoku.ac.jp

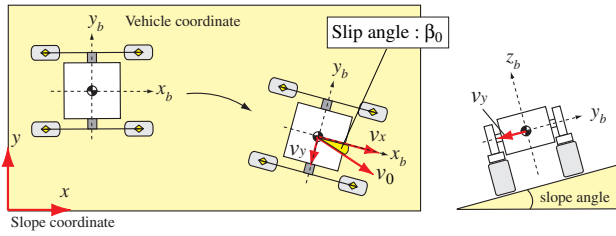


Fig. 1. Definition of slip angle of vehicle

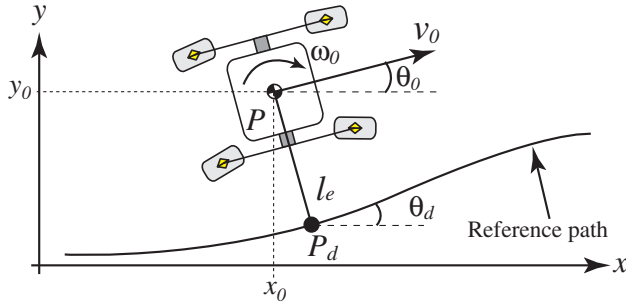


Fig. 2. Illustration of path following (w/o sideslip)

wheel slippages. The wheel slippage can be divided into the longitudinal and lateral slips. A key issue in our proposed control is the compensation of these three slips while the rover follows an arbitrary path.

A general illustration of the path following problem is shown in Fig. 2. In the path following problem, a feedback control law is employed to reduce both distance and orientation errors. The distance error, denoted by l_e , is determined as a distance between P and P_d . The orientation error, θ_e , is given as $\theta_0 - \theta_d$. Here, θ_0 is a vehicle orientation around yaw-axis of the vehicle. θ_d is the angle between the x-axis of the inertial coordinate system and the tangent to the path at P_d (vehicle's desired orientation).

Referring to conventional path following algorithm, a vehicle is controlled such that the vector of linear velocity of the vehicle v_0 coincides with a tangent of a given path as shown in Fig. 3-(a). The slip angle of vehicle in this case is assumed to be negligible, and therefore, the conventional control has been verified in slip-less condition. However, as shown in Fig. 3-(b), if the vehicle experiences its sideslip with a certain amount of slip angle β_0 , this slip angle becomes an additional orientation error even when the vector of vehicle velocity is in line with the path. From the above statement, the orientation error for path following control in high slip environment should be defined as a combination of both pure orientation error θ_e and slip angle β_0 .

B. Slip Compensation Control with Path Following

As noted above, a feedback control law for path following is employed to satisfy both zero distance and zero orientation errors. In this research, we consider that the orientation error separately consists of two different angles, $\theta_e (= \theta_0 - \theta_d)$ and β_0 . If the orientation error is dealt with a set of them, namely $\theta_e = \theta_0 + \beta_0 - \theta_d$, the vehicle orientation cannot reach a desired orientation θ_d . Therefore, the control objectives

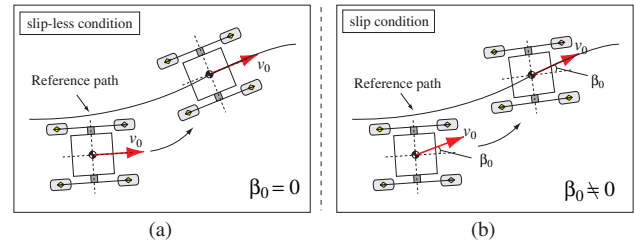


Fig. 3. path following problem w/ and w/o slip angle of vehicle

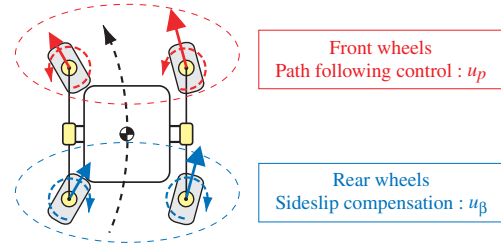


Fig. 4. Approach of slip compensation control with path following

in our proposed control can be defined as, $l_e \rightarrow 0$, $\theta_e \rightarrow 0$, and $\beta \rightarrow 0$. These control objectives are achieved by using one control variable, which is a turning angular velocity of vehicle ω_0 .

Considering a linear state feedback control when v_0 is not to be zero, a desired control variable u_p for a path following task is give by:

$$u_p = -k_1 v_0 l_e - k_2 |v_0| \theta_e - k_3 |v_0| \dot{\theta}_e \quad (2)$$

where, k_1 , k_2 , and k_3 are control gains.

Another desired control variable u_β for a sideslip compensation is modeled by the following equation:

$$u_\beta = k_4 \beta_0 - k_5 |v_0| \theta_e - k_6 |v_0| \dot{\theta}_e \quad (3)$$

where, k_4 , k_5 , and k_6 are control gains.

A key issue here is how to manage these two different control inputs, in order to fulfill the both path following and slip compensation controls. We tried to several combinations of them, and then elaborated upon the following approach: as shown in Fig. 4, the front wheels of the rover work to follow a path using u_p , while rear wheels compensate the vehicle's sideslip based on u_β . These two control variable, u_p and u_β , are executed by both steering and driving maneuvers as formulated later in Section III. Note that, these maneuvers compensate remaining concern in wheel slips.

III. DERIVATION OF STEERING AND DRIVING MANEUVERS

Both the path following task and sideslip compensation are practically accomplished by the several actuators that are located on steering and driving units of rover. Therefore, we have proposed how to distribute the control inputs to both steering and driving axes with consideration of the wheel slips as in [9]. In order to derive appropriate maneuvers, nonholonomic constraints of a four-wheeled vehicle including the vehicle's sideslip and the lateral slip of wheel are

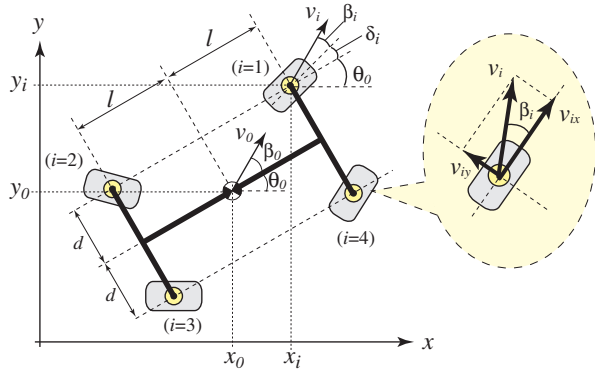


Fig. 5. Kinematic model of four-wheeled vehicle

employed. Controlling the angular velocity of each driving axle also compensates the longitudinal slip of wheel.

A. Nonholonomic Kinematic Model of Vehicle

To discuss the nonholonomic kinematic model, the following assumptions are considered: 1) the distance between wheels (generally called wheelbase and tread) are strictly fixed; 2) the steering axle of each wheel is perpendicular to the terrain surface; 3) the vehicle does not consist of any flexible parts.

1) *Kinematic model with slip angle*: A kinematic model of a four-wheeled vehicle including the slip angle of vehicle and lateral slips of wheel is shown in Fig. 5. In this model, each wheel has a steering angle δ_i and slip angle of wheel β_i . The slip angle of wheel, which measures a wheel lateral slip, is calculated by same equation as (1) using the longitudinal and lateral linear velocities of wheel, v_{ix} and v_{iy} , as follows:

$$\beta_i = \tan^{-1}(v_{iy}/v_{ix}) \quad (4)$$

The subscript i denotes the wheel ID as shown in Fig. 5.

The position and orientation of the center of gravity of the vehicle is defined as (x_0, y_0, θ_0) , while (x_i, y_i) gives the position of each wheel. v_i is the linear velocity of each wheel. l is the longitudinal distance from the center of gravity of the vehicle to the front or rear wheel and d defines the lateral distance from the center of gravity of the vehicle to the left or right wheel. Here, based on previously defined assumptions, l and d are constant values.

2) *Nonholonomic constraints*: The nonholonomic constraints are expressed by the following equation, taking into account the lateral slip:

$$\dot{x}_0 \sin \phi_0 - \dot{y}_0 \cos \phi_0 = 0 \quad (5)$$

$$\dot{x}_i \sin \phi_i - \dot{y}_i \cos \phi_i = 0 \quad (6)$$

where, $\phi_0 = \theta_0 + \beta_0$, and $\phi_i = \theta_0 + \delta_i + \beta_i$.

Further, geometric constraints between every wheel and the center of gravity of the vehicle are written as:

$$\left. \begin{aligned} x_1 &= x_0 + l \cos \theta_0 - d \sin \theta_0 \\ x_2 &= x_0 - l \cos \theta_0 - d \sin \theta_0 \\ x_3 &= x_0 - l \cos \theta_0 + d \sin \theta_0 \\ x_4 &= x_0 + l \cos \theta_0 + d \sin \theta_0 \end{aligned} \right\} \rightarrow x_i = x_0 + X_i \quad (7)$$

$$\left. \begin{aligned} y_1 &= y_0 + l \sin \theta_0 + d \cos \theta_0 \\ y_2 &= y_0 - l \sin \theta_0 + d \cos \theta_0 \\ y_3 &= y_0 - l \sin \theta_0 - d \cos \theta_0 \\ y_4 &= y_0 + l \sin \theta_0 - d \cos \theta_0 \end{aligned} \right\} \rightarrow y_i = y_0 + Y_i \quad (8)$$

It is obvious that X_i and Y_i describe the distances between every wheel and the center of gravity of the vehicle.

B. Steering Maneuvers

To elaborate upon the desired steering angle of each wheel, first, by transforming the nonholonomic constraints, (6), we obtain the following:

$$\delta_{di} = \tan^{-1}(\dot{y}_i/\dot{x}_i) - \theta_d - \beta_i \quad (9)$$

Subsequently, substituting (7) and (8) into (9), δ_{di} is derived by the following equation:

$$\delta_{di} = \tan^{-1} \left(\frac{v_d \sin \theta_d - \dot{Y}_i(\dot{\theta}_d)}{v_d \cos \theta_d - \dot{X}_i(\dot{\theta}_d)} \right) - \theta_d - \beta_i \quad (10)$$

where, v_d represents the desired linear velocity of vehicle and $\dot{\theta}_d$ is the desired turning angular velocity of vehicle. As described in Section II, the control objectives are achieved by a turning angular velocity. Therefore, $\dot{\theta}_d$ can be finally given the following equations to satisfy the control objectives:

$$\dot{\theta}_d = \begin{cases} u_p : -k_1 v_0 l_e - k_2 |v_0| \theta_e - k_3 |v_0| \dot{\theta}_e & (\text{front wheels}) \\ u_\beta : k_4 \beta_0 - k_5 |v_0| \theta_e - k_6 |v_0| \dot{\theta}_e & (\text{rear wheels}) \end{cases} \quad (11)$$

C. Driving Maneuvers

The driving maneuver is achieved by the control of the wheel's angular velocity ω_i . The relationship between ω_i and wheel's linear velocity v_i can be written as:

$$\omega_i = v_i \cos \beta_i / r \quad (12)$$

where, r is wheel radius. Here, v_i can be expressed by \dot{x}_i or \dot{y}_i :

$$v_i = \dot{x}_i / \cos \phi_i = \dot{y}_i / \sin \phi_i \quad (13)$$

Substituting (7) or (8) into the above equations, the desired angular velocity of the wheel ω_{di} can be finally derived:

$$\omega_{di} = \begin{cases} (v_d \cos \theta_d + \dot{X}_i(\dot{\theta}_d)) \cos \beta_i / r \cos \phi_i & (\theta_d \leq \pi/4) \\ (v_d \sin \theta_d + \dot{Y}_i(\dot{\theta}_d)) \cos \beta_i / r \sin \phi_i & (\theta_d \geq \pi/4) \end{cases} \quad (14)$$

Additionally, ω_{di} has to be adjusted to compensate the longitudinal slip of wheel. The slip in the longitudinal direction is measured by *slip ratio* s_i , which is calculated as a function of the longitudinal linear velocity v_{ix} and the circumference velocity of the wheel $r\omega_i$:

$$s_i = \begin{cases} (r\omega_i - v_{ix}) / r\omega_i & (r\omega_i > v_{ix} : \text{driving}) \\ (r\omega_i - v_{ix}) / v_{ix} & (r\omega_i < v_{ix} : \text{braking}) \end{cases} \quad (15)$$

The slip ratio assumes a value in the range from -1 to 1 .

Therefore, an improved desired angular velocity $\hat{\omega}_{di}$ compensating the longitudinal slip is rewritten as follows:

$$\hat{\omega}_{di} = \omega_{di} / (1 - (s_{ref} - s_i)) \quad (16)$$

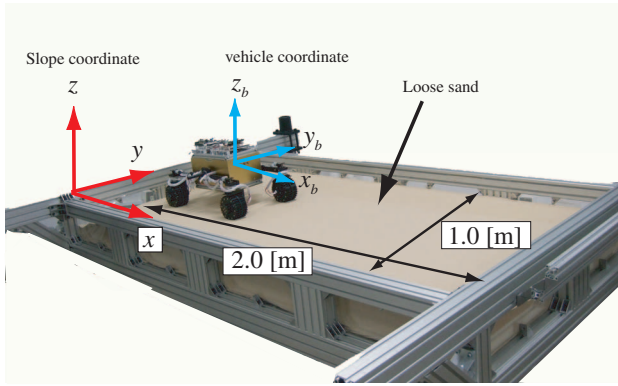


Fig. 6. Overview of the experimental setup

where, s_{ref} represents the reference slip ratio to regulate the longitudinal slip of wheel. In our approach, the value of s_{ref} is given between 0.1 and 0.3, where the most efficient value of a wheel traction is obtained comparing to our previous researches.

IV. SLOPE TRAVERSAL EXPERIMENTS

In order to verify the proposed control, slope traversal experiments were carried out using a rover test bed developed in our research group. In particular, to generate larger dynamic slip motions of the rover, we conducted the experiments on the side slope traversal situation using a tiltable test field. The performance of the proposed control is evaluated based on the distance and orientation errors.

A. Experimental Setup

Fig. 6 shows the overview of the experimental setup with our rover test bed on the tiltable test field. The test field consists of a flat rectangular soil-vessel in the size of 2.0 by 1.0 [m]. The vessel is filled up with 8.0 [cm] depth of a *Toyoura Sand*, which is loose sand and standard sand for terramechanics research filed. The vessel can be inclined up to 20 [deg].

1) *Rover test bed*: The four-wheeled rover test bed as shown in Fig. 7 has a dimension of 0.44 [m] (wheelbase) \times 0.30 [m] (tread) \times 0.30 [m] (height) and weights about 13.5 [kg] in total. Each wheel of the rover has a diameter of 10 [cm] and a width of 6.4 [cm], and it is covered with paddles having a height of 0.5 [cm]. Every wheel can steer in the range of ± 90 [deg]. An on-board computer located inside of the rover executes all steering and driving maneuvers based on the proposed slip compensation control.

2) *Measurement system for velocity and orientation*: Measurement of the slip motions is the key procedure to achieve the proposed control. As defined in (1), (4), and (15), the slip motion can be calculated by the velocities of vehicle/wheel. There are several approaches to measure the velocity of vehicle: for example, using an IMU (Inertial Measurement Unit), LMS (Laser Measurement Systems) or visual sensors. Since the scope of this research is to evaluate the effectiveness of the slip compensation control, the velocity measurement in the experiment should not include any errors and deviations. Therefore, we employed a

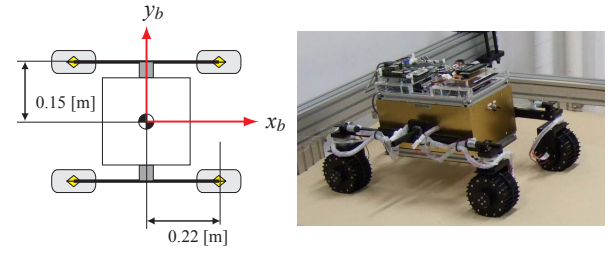


Fig. 7. Rover test bed

TABLE I
CONTROL GAINS AND DESIRED VALUES

k_1	k_2	k_3	k_4	k_5	k_6	θ_d [deg]	v_d [cm/s]
10.0	2.0	0.30	0.10	2.0	0.30	0.0	4.5

motion capture camera (Stereo Labeling Camera, developed by CyVerse corp.) which can measure corresponding position of a reflection maker mounted on the center of gravity of the rover. This stereo camera is fixed on the tripod stand and the direction of the camera is set such that the camera can perfectly look down upon the test field. The velocity of the rover, therefore, can be calculated by the derivative of the time history of the position data.

The vehicle orientations for roll and pitch axes are measured by two inclinometers fixed to each axis of the rover. Another orientation around yaw axis is also calculated by integration of an angular velocity data taken by a gyroscope mounted on the rover.

B. Experimental Condition

The set of experiments were conducted in three cases by changing the slope angle of the tiltable field from 5.0 [deg] to 10 [deg] in steps of 2.5 [deg]. In each slope angle, the test run was conducted in twice. The reference path to be followed was given as a straight path along with the side slope traversal direction.

In the case of the control with slip compensation, the control variable for the path following u_p was distributed into steering/driving axels on front wheels, while u_β was to those on rear wheels to compensate the sideslip. The control gains and desired values are summarized in Table I. On the other hand, in the case of the no-control, every steering angle was fixed to maintain the angle of 0 [deg] and every wheel was controlled to maintain constant velocity of 0.9 [rad/sec].

C. Experimental Procedure

The experimental procedures are summarized as follows:

- 1) Set the rover on the experimental field (at this time, every steering angle is fixed as 0 [deg].).
- 2) Capture the initial position of the rover by using the stereo camera, and then make the rover start moving.
- 3) Measure the velocity and orientation of the rover.
- 4) Calculate the distance and orientation errors, slip ratio and slip angle of every wheel, and the slip angle of vehicle.

- 5) Determine the path following and slip compensation inputs, based on (2) and (3).
- 6) Derive the steering and driving maneuvers by using (10) and (16).
- 7) Input calculated maneuvers to steering and driving axles.
- 8) return to 3).

The above control sequence from 3) to 8) were executed every 0.5 [sec].

D. Experimental Result

The experimental results for the motion traces of the rover are shown in Fig. 8-(a), (b), and (c). Fig. 9 describes the snapshots when the rover traversed a slope of 10 [deg] with and without the slip compensation control. Further, errors in distance and orientation ($= \theta_0 + \beta_0$) are summarized in Table II. The errors are evaluated by both root mean square (rms) and final state errors. The error percentage for the distance is calculated by dividing the error value by the length of the reference path.

From the results of the motion traces, it can be clearly seen that the rover with slip compensation control can successfully follow the reference path in every slope angle. In particular, it must be emphasized that the distance errors are in a negligible order since each error value is almost equal to the sensor accuracy of the stereo labeling camera. The orientation errors are also controlled less than a few degrees. Also, repeatability of the experiment in each slope angle case can be confirmed based on Fig. 8 and error values as summarized in Table II.

Throughout the experiments, it was observed that the slip ratios dynamically changed in the range of -0.3 to 0.8, and also, the slip angles were approximately in the range of -45 [deg] to 55 [deg] in no control case. Despite such dynamic slip motions, the proposed slip compensation control enables the rover to maneuver with appropriate counter-steering/driving motions and then follow an arbitrary path even in the slope traversal situation on loose sand. Comparing to the result of no control case, the errors are successfully reduced by applying the slip compensation control

E. Discussion for Enhancement of Controller

The authors would like to make brief comments on the following three issues for further discussion, which are 1) on-board measurement of rover's position/velocity, 2) tuning of controller gains, and 3) introduction of a feedforward loop.

In the experiments presented in this paper, the authors employed an external stereo camera fixed to the environment for the measurements of the position and traveling velocity of the rover, and used these information in the path following and slip compensation controls. This has significantly made it easy to demonstrate reliable performance of the proposed control. However in practical cases, these measurements should be done by on board sensors. Inertial sensors such as accelerometers, or vision-based sensors such as a stereo camera, or combination of these with an appropriate filtering technique are common approach to this issue. In addition, for the direct measurement of the traveling velocity of the

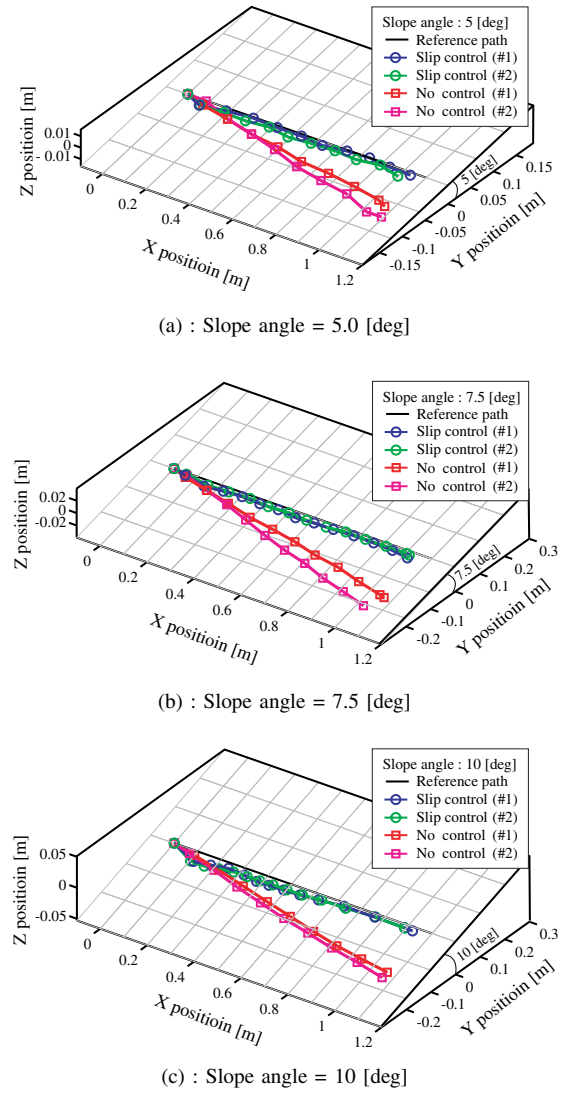


Fig. 8. Motion traces of the rover

rover, visual odometry has been recently studied well as a promising method. Applying this technique, we have been developing a visual odometry system to measure the velocity in order to achieve the slip compensation control with full-on-board systems.

The second issue is on the performance of the controller. As observed in Table II, path following performance for orientation is not equivalent to that for distance. This is deduced due to imperfect setting of the gains for orientation error. As defined in (2) and (3), it is obvious that the proposed control consists of P feedback control for distance error and PD feedback control for orientation error. Therefore, from the experiments, we could observe different motion behaviors with the different control gains. Note that, the controller gains in the experiment were given as fixed values for all cases for fair comparison, but for the better performance they could be adjusted along with the slope angle, terrain characteristics, and the shape of the reference paths.

The third issue is for the improvement of the controller

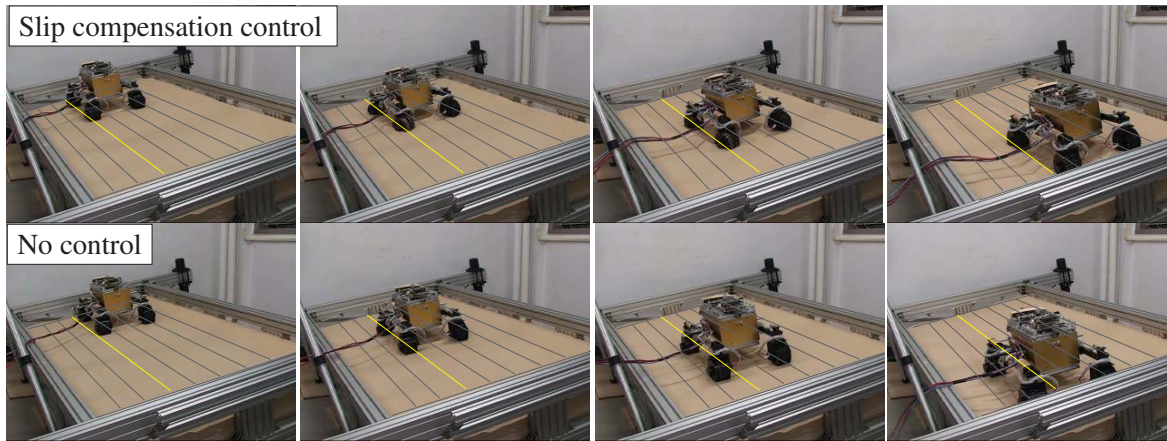


Fig. 9. Snapshots of the slope traversal experiments, slope angle = 10 [deg] (above : Slip compensation control, below : No control)

TABLE II
PATH FOLLOWING ERRORS

Slope angle [deg]	w/ slip compensation control				No control			
	Orientation error [deg]		Distance error [m]		Orientation error [deg]		Distance error [m]	
	rms	Final state	rms	Final state	rms	Final state	rms	Final state
5.0 (#1)	5.61	3.76	0.005 (0.47 %)	0.002 (0.21 %)	6.27	7.42	0.045 (4.20 %)	0.074 (6.99 %)
(#2)	5.54	2.99	0.011 (1.03 %)	0.015 (1.46 %)	6.72	0.23	0.057 (5.22 %)	0.094 (8.65 %)
7.5 (#1)	5.65	0.13	0.015 (1.43 %)	0.015 (1.49 %)	9.95	11.80	0.096 (9.02 %)	0.163 (15.29 %)
(#2)	5.08	3.27	0.012 (1.19 %)	0.013 (1.25 %)	12.03	9.20	0.125 (12.17 %)	0.208 (20.29 %)
10.0 (#1)	6.47	2.03	0.020 (1.91 %)	0.012 (1.15 %)	13.23	5.10	0.096 (8.58 %)	0.157 (13.97 %)
(#2)	6.59	2.33	0.021 (2.02 %)	0.010 (1.00 %)	9.43	6.18	0.110 (9.61 %)	0.177 (15.48 %)
Average	5.82	2.41	0.014 (1.34 %)	0.011 (1.09 %)	9.61	6.66	0.088 (8.13 %)	0.146 (13.45 %)

performance. As observed in Fig. 8, the rover experienced relatively large distance error in initial few centimeters because the path following and slip compensation control starts working only after the system detects any errors in position or orientation.

This is due to the nature of the “control delay of feedback”, but if a “feedforward” loop is added in the controller with a good prediction on the slip motion of the rover, the control performance will be improved significantly.

These last two issues, the better tuning of feedback gains and the introduction of a feedforward loop, are closely related each other in a sense that a terramechanics-based model on the wheel slippages could be useful to improve the performances. Eventually, the present authors have developed a substantial model for the wheel slippage on loose soil [8], such background knowledge will be applied to determine the feedback gains and feedforward signals to each wheel, depending on terrain characteristics, slope angles and slip conditions.

V. CONCLUSION AND FUTURE WORKS

In this paper, the usefulness of the slip compensation control with path following developed in our previous work has been confirmed through the slope traversal experiments. Based on the proposed approach, the rover could make appropriate steering and driving maneuvers to follow a given path with sufficient accuracy as well as to reduce the sideslip of the rover, even in high slip environment. The effectiveness of the proposed control has been verified by quantitative evaluations of distance and orientation errors. Comparing to other path following methods, advantages of the slip

compensation control developed in this work are summarized as follows: 1) vehicle sideslip and wheel longitudinal/lateral slips are completely included into the control maneuver, 2) controls for path following and slip compensation are respectively fulfilled by giving different control inputs to front/rear wheel pairs, and 3) the control approach can be applied to any situations in varying types of soils.

Subsequently, the issues for the enhancement of the control performance, such as better tuning of feedback gains and introduction of a feedforward loop, have been discussed based on the experimental results.

REFERENCES

- [1] M. Maimone, Y. Cheng, and L. Matthies; “Two Years of Visual Odometry on the Mars Exploration rovers,” *Journal of Field Robotics*, vol. 24, no. 3, pp.169-186, 2007.
- [2] A. De Luca, G. Oriolo, and C. Samson; *Robot Motion Planning and Control*, edited by J.-P. Laumond, Springer-Verlag, 1998.
- [3] S. Rezaei, J. Guivant and E. M. Nebot; “Car-Like Robot Path Following in Large Unstructured Environments,” *Proc of the 2003 IEEE Int. Conf. on Intelligent Robots and Systems*, 2003, pp. 2468-2473.
- [4] D. M. Helmick et al.; “Slip-compensated path following for planetary exploration rovers,” *Advanced Robotics*, Vol. 20, No. 11, 2006, pp. 1257-1280.
- [5] M. G. Bekker; *Introduction to Terrain-Vehicle Systems*, The University of Michigan Press, 1969.
- [6] J. Y. Wong; *Theory of Ground Vehicles*, John Wiley & Sons, 1978.
- [7] K. Iagnemma and S. Dubowsky; *Mobile Robot in Rough Terrain*, Springer Tracts in Advanced Robotics, vol.12, 2004.
- [8] G. Ishigami, A. Miwa, K. Nagatani, and K. Yoshida; “Terramechanics-Based Model for Steering Maneuver of Planetary Exploration Rovers on Loose Soil,” *The Journal of Field Robotics*, Vol. 24, No. 3, pp. 233-250, 2007.
- [9] G. Ishigami, K. Nagatani, and K. Yoshida; “Path Following Control with Slip Compensation on Loose Soil for Exploration Rover,” *Proc. of the 2006 IEEE Int. Conf. on Intelligent Robots and Systems*, 2006, pp. 5552-5557.